Journal of Materials Chemistry A

Accepted Manuscript

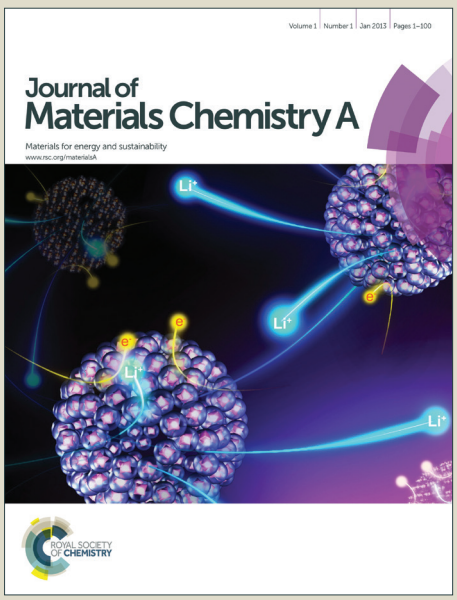

ROYAL SOCIETY OF CHEMISTRY

www.rsc.org/materialsA

Journal of Materials Chemistry A RSCPublishing

COMMUNICATION

Retransformed graphitic activated carbon from an ionic liquid-derived nitrogen containing carbon

Cite this: DOI: 10.1039/x0xx00000x

Mok-Hwa Kim,[a,b] Sol Yun,[d] Ho Seok Park,*[d] Joong Tark Han,[c] Kwang-Bum Kim,[b] and Kwang Chul Roh*[a]

Received ooth January 2014,
Accepted ooth January 2014

DOI: 10.1039/x0xx00000x

www.rsc.org/

The carbonization and chemical activation of an ionic liquid are demonstrated to produce an outstanding structural combination of an unexpectedly high surface area and a graphitic structure. This activated carbon has a very high CO_2 uptake and high specific capacitance, thus making it ideally suited to advanced energy storage systems.

Carbon materials have attracted considerable interest due to their high diversity in terms of crystallinity, morphology, porosity and texture, as well as the ease with which these characteristics can be manipulated to fulfill specific application requirements. Among the various carbon materials available, porous carbon provides a unique combination of high specific surface area and large pore volume in addition to excellent chemical and mechanical stability. These structural peculiarities play a particularly important role in sorption, catalysis, gas storage, sensing and energy storage systems; such applications being very much dependent on the pore structure, surface composition and micromorphology of the carbon.[1–6]

As a source for porous carbon, ionic liquids (ILs) have received a great deal of attention recently due to the significant advantages they offer. The importance of ILs as a carbon source was recognized quite early on, and has since led to numerous studies into their chemical and physical properties, as well as their potential applications. Of particular interest are functionalized ILs that contain tertiary nitrogen in their cation, as these have the potential to react with CO_2 to form carbamate species that can be considered an activated form of CO_2.[7] However, despite ILs being well established as precursors for a variety of compounds, they have only very recently been used as a precursor for the N-modification of carbon materials.[7–10]

Owing to the presence of nitrogen-containing cations such as 1-ethyl-3-methylimidazolium (EMIM), and cyano-functionalized anions such as dicyanamide (dca) or tricyanomethide (tca), carbon materials derived from an IL typically feature sp^2-hybridized carbons and can be graphitized at higher temperatures than conventional carbonization.[11] More importantly, thanks to the inevitable nitrogen heteroatoms contained within their structure, they are not decomposed completely under thermal treatment in an inert gas atmosphere. Indeed, most researchers have focused on this particular feature, as it allows for the fabrication and processing of functional carbon. Nevertheless, there does not appear to have been any reports of IL-derived activated carbon being used as an electrode material in supercapacitors or for the adsorption of CO_2, the only exceptions being the use of functionalized carbon materials as a hard template and the nitrogen modification of carbon sources.[8–10] Looking at this from a new perspective, we have instead focused on the structural changes that occur when nitrogen is removed from an IL-derived carbon structure. We therefore herein report the first IL-derived activated carbon (IL-AC) to be prepared by carbonization and chemical activation. It is interesting to note that the nitrogen-containing carbon structure of the carbonized materials (IL-C) could be retransformed to a graphitic activated carbon; and to the best of our knowledge, this is the first demonstration of IL-AC with a nanoporous and graphitic structure suitable for both supercapacitors and CO_2 adsorption. We also investigated the correlation between these structural changes and the chemical activation of the carbonized materials.

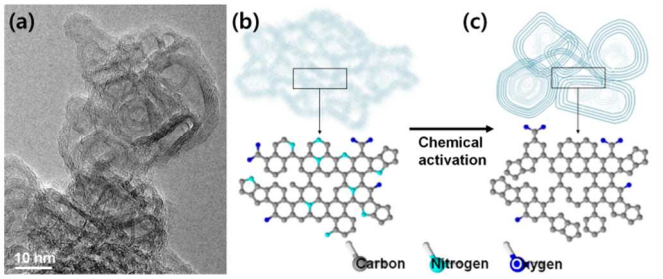

Fig. 1 The synthesis of ionic liquid-derived activated carbon (IL-AC). (a) HRTEM image of IL-AC showing the presence of torispherical carbon. Schematic illustration of the structural changes induced by (b) carbonization and (c) chemical activation. Note that the resultant product forms a highly nanoporous and partially graphitic structure

The present fabrication strategy is therefore based on a carbonization and chemical activation processes that uses EMIM-dca as the precursor, resulting in a highly nanoporous and partially graphitic structure (Fig 1a). A schematic illustration of this structural change via carbonization and chemical activation is given in Fig. 1b and 1c. Although IL-C may contribute to the formation of graphitic features to some extent, we do not believe that this is solely responsible for the crystalline structure. Instead, it is thought that the exclusion of nitrogen contributes to the partial collapse of the overall structure, leading to a graphitic structure and nanopores in the IL-AC.

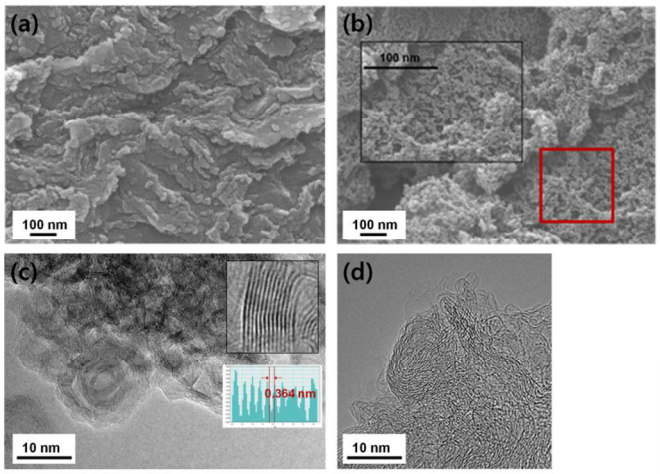

Fig. 2 Change in the surface morphology and microstructure of activated carbon. (a) FE-SEM image of IL-C. (b) FE-SEM image of IL-AC. The inset represents the area outlined by the red square. (c) HRTEM image of IL-AC showing its polyhedral carbon structure with nanopores. The inset shows an expanded view of its graphitic structure and the 0.36 nm spacing of its lattice planes obtained through direct line scanning analysis. (d) STEM image of IL-AC.

Subsequent field-emission scanning electron microscopy (FE-SEM) analysis of IL-C (Fig. 2a) revealed an irregular and non-porous surface morphology that is in stark contrast to the highly porous surface of IL-AC (Fig. 2b). The inset in Fig. 2b also shows that the size of these nanopores ranges from 2 to 10 nm, and that they exhibit a low degree of order. The difference in microstructure between IL-C and IL-AC was further examined by high-resolution transmission electron microscopy (HRTEM) and Cs-corrected scanning tunneling electron microscopy (STEM), revealing a highly bent graphitic microstructure in IL-C (Fig. S1, ESI†) that contains curved microdomains with no long-range order, and only very weak edge termination. In contrast, we can clearly see evidence of polyhedral carbon in IL-AC (Fig. 2c), with the curving of the graphite layers to form closed graphite structures suggesting the presence of torispherical carbon. From the direct line scanning analysis shown in the inset of Fig. 2c, the lattice plane spacing was determined to be 0.364 nm. Much like the HRTEM analysis, the STEM image of IL-C reveals a graphitic structure with limited extension in bent microdomains, whereas IL-AC shows a graphitic microstructure with long-range order (Fig. 2d). This can be explained by the penetration of potassium into the carbon structure during chemical activation and subsequent removal of nitrogen and hydrogen, which results in the non-edged structures identified in IL-C being rearranged into the polyhedral carbon structure seen in IL-AC. Consequently, IL-AC is expected to provide an alternative route to developing advanced carbon materials.

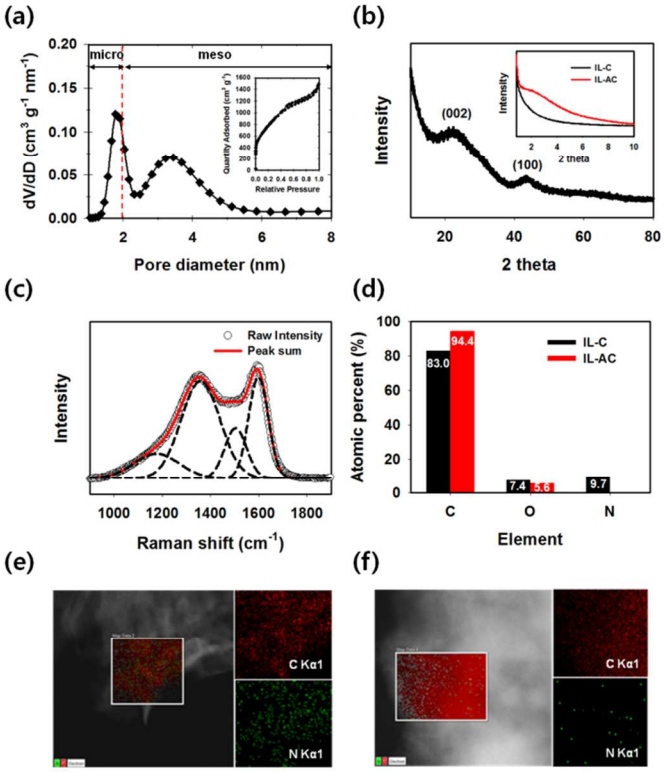

Fig. 3 (a) Pore size distribution curves of IL-AC, as determined by NLDFT model. IL-AC possesses pores that are mostly in the micropore (centered at 1.8 nm) and mesopore (centered at 3.2 nm). Nitrogen adsorption-desorption isotherms of IL-AC shown in the inset of a. (b) XRD pattern of IL-AC showing the characteristic carbon (002) and (100) planes. Low angle XRD patterns for IL-C and IL-AC in the inset of b, showing their difference in pore structure. (c) Raman spectra of IL-AC. Deconvoluted peaks of materials shows four Gaussian sub-bands. (d) XPS elemental analysis results showing the disappearance of nitrogen from IL-AC after chemical activation. Elemental maps of (e) IL-C and (f) IL-AC showing widespread distribution of carbon (red) and nitrogen (green) in IL-C, but very little evidence of nitrogen in IL-AC.

Fig. 3a shows the pore size distribution (PSD) curve obtained using a non-local density functional theory (NLDFT) model, which demonstrates that IL-AC possesses mostly micropores (centered at 1.8 nm) and mesopores (centered at 3.2 nm).[12,13] The nanoporous nature of IL-AC is also confirmed by its nitrogen adsorption-desorption, which as shown by the combined type-I/IV nitrogen isotherm in the inset of Fig. 3a, reveals a high specific surface area of 2823 m^2 g^{-1}.[13–15] In contrast, IL-C exhibits a type-IV nitrogen sorption isotherm with a specific surface area of 4 m^2 g^{-1} (Fig. S2(a), ESI†), while the PSD derived using NLDFT shows mostly meso and macropores (Fig. S2(b), ESI†). The marked hysteresis evident in this nitrogen adsorption data confirms the presence of mesopores in both materials; however, the greater specific surface area and pore volume of IL-AC could be attributed to chemical activation.[3]

Moreover, the strong nitrogen adsorption of IL-AC at low pressure, and its slightly steep adsorption at a relative pressure of 0.8-1.0, shows that micro/mesopores coexist despite the huge increase in pore volume (2.3 cm^3 g^{-1}).[14] This not only indicates that these materials have great potential for CO_2 adsorption, but such pore characteristics can also be expected to provide an electrode/electrolyte interface area sufficient for the accumulation of ions in supercapacitor applications.

In the X-ray diffraction (XRD) results given in Fig. 3b, it is clear that the (002) peak of IL-AC has a markedly reduced intensity and is dramatically broadened when compared to the equivalent peak for IL-C (Fig. S2(c), ESI†). This indicates that the average interlayer distance increases from 0.34 to 0.36 nm in IL-AC, thus confirming that it is indeed etched by chemical activation. This mesoporous structure was further investigated by low-angle XRD (inset in Fig. 3b), in which the broad characteristic diffraction peak of IL-AC at about 2.0° is characteristic of a weakly mesoporous structure with no long-range order.[15] In contrast, the IL-C sample exhibits a non-ordered mesoporous structure, which agrees well with the FE-SEM results.

Fig. 3c shows the Raman spectra and deconvoluted peaks of IL-AC with four Gaussian sub-bands, in which we see the characteristic D-band representing the disorder of graphite edges appear along with the active E_{2g} phonon G-band at ~1360 cm^{-1} and ~1600 cm^{-1}, respectively. The evidence of a broad band at 1150–1200 cm^{-1} implies the presence of functional groups such as C=O, whereas the wide peak at ~1500 cm^{-1} is characteristic of amorphous sp^2-bonded carbon.[17,18] The Raman spectrum for IL-C is given in Fig. S2(d, ESI†), and shows the same four Gaussian sub-bands as IL-AC. There is, however, a difference in their respective relative integrated intensities of the D-band relative to the G-band (I_D/I_G), which represents the degree of disorder in the graphite structure and was estimated to be 2.71 for IL-C and 1.89 for IL-AC. The amount of amorphous carbon relative to graphite can also be estimated from the integrated intensity ratio of 1500 cm^{-1}/1600 cm^{-1}, which equates to 2.16 for IL-C and 0.56 for IL-AC.[18] This clearly indicates that IL-C has a certain degree of structural disorder and amorphous content when compared with IL-AC, but this directly contradicts the XRD results. It can therefore be concluded that IL-AC is affected by chemical activation in a way that not only increases its disorder by creating a highly nanoporous structure, but also introduces a graphitic structure by restructuring the carbon atoms.

Further information regarding the atomic composition of each material was obtained by X-ray photoelectron spectroscopy (XPS) analysis, based on which the atomic percentages of carbon, nitrogen and oxygen are given in Fig. 3d. Interestingly, although IL-C clearly contains carbon, nitrogen and oxygen, the XPS spectrum of IL-AC only exhibits peaks corresponding to carbon and oxygen. This was further confirmed by energy-dispersive X-ray spectroscopy (EDS) mapping, with the results for IL-C in Fig. 3e clearly showing the distribution of both carbon (red) and nitrogen (green), but very little evidence of nitrogen in IL-AC (Fig. 3f). This indicates that nitrogen was removed during chemical activation, suggesting that the graphitic structure in IL-AC is caused by a dramatic restructure of carbon due to the removal of nitrogen.

In order to further evaluate the gas storage capacity of IL-AC, its high-pressure adsorption capacity of CO_2 was measured at 298 K and 1,100 kPa. As can be clearly seen in Fig. 4a, IL-AC exhibits a very high CO_2 adsorption capacity of 10.2 mmol g^{-1} that can be mainly ascribed to its microporosity and high specific surface area.[5,6] Moreover, this value is comparable to the commercial AC that contains microporous structure.

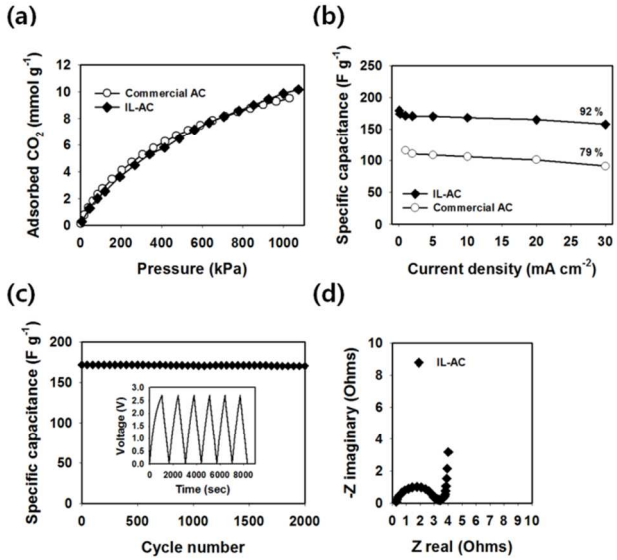

Fig. 4. (a) CO_2 adsorption isotherms for IL-AC and commercial AC at 298 K. (b) Specific capacitance versus current density for IL-AC and commercial AC s. (c) Cycle performance of IL-AC. Constant-current cycles were run at a rate of 1 mA cm^{-2}. A capacity retention of 99 % was obtained after 2,000 cycles. (d) Electrochemical impedance plot of an IL-AC electrode recorded across a frequency range of 100 kHz to 100 mHz.

To evaluate the potential of IL-AC for use as an electrode material, it was used to assemble a two-electrode system for a supercapacitor. The resulting cyclic voltammetry (CV) profile (Fig. S4, ESI†) retains a near-rectangular shape at all sweep rates between 5 and 20 mV s^{-1}. More importantly, however, IL-AC exhibits a near-rectangular shape at high sweep rates, which is indicative of typical capacitive behavior with good charge propagation and easy ion transport in the electrode material. As shown in Fig. 4b, the rate performance was assessed through plots of specific capacitance versus current density for devices based on either IL-AC or commercial activated carbon (AC). From this, the specific capacitance achieved with IL-AC was calculated to be 180, 174 and 172 F g^{-1} at current densities of 0.1, 0.2 and 1.0 mA cm^{-2}, respectively.[3] Note that despite this decrease in specific capacitance with increasing current density, 92 % of the capacitance at 1.0 mA cm^{-2} is still retained at 30 mA cm^{-2}; a result which shows a consistently higher specific capacitance at increased current density than commercial AC. Since a loss of specific capacitance is usually related to problems of kinetics at the electrode, this increase indicates that IL-AC can more rapidly generate an electrical double layer on its surface. This can be attributed to the unique structure of IL-AC, wherein the combination of micro/mesopores and a graphitic

structure improves the ion diffusion rate and provides very good electrical conductivity.[3,4,19] Fig. S5 (ESI†) reveals IL-C to be an electrochemically inactive material for supercapacitors because of its low specific surface area and an almost non-porous structure. This material also exhibited a very stable cycle performance (Fig. 4c), with only a slight loss of capacitance after 2,000 cycles at a current density of 1.0 mA cm^{-2}, and a retained Coulombic efficiency of more than 99 %. The impedance spectrum acquired, shown as a Nyquist plot in Fig. 4d, exhibits a typical arc in the high-frequency region and a spike in the low-frequency region. Notably, this plot shows an almost vertical line at low frequencies, which is indicative of highly capacitive behavior.[20] The superior rate capability and excellent capacitive behavior of IL-AC can be attributed to effective reaction on its surface and the high electrical conductivity of the electrode.

In conclusion, this study has demonstrated that activated carbon produced from an ionic liquid (EMIM-dca) through carbonization and chemical activation offers a unique combination of high surface area through micro/mesopores and a graphitic structure that provides good electrical conductivity. These properties are attributed to the removal of nitrogen, which causes a rearrangement of atoms to create a new structure. When used as a supercapacitor electrode, this so-called IL-AC material can achieve a high specific capacitance, outstanding rate capability and excellent cycling stability. It is therefore believed that this material has great potential for future practical application in high-power energy storage systems.

This work was supported by an Energy Efficiency and Resources grant from the Korea Institute of Energy Technology Evaluation and Planning (KETEP), as funded by the Korean Government's Ministry of Knowledge Economy (No: 20122010100090).

Notes and references

[a] Energy & Environmental Division, Korea Institute of Ceramic & Engineering & Technology, Seoul 153-801, Republic of Korea. Fax: (+82) 2 3282 2475; Tel: (+82) 2 3282 2463; E-mail: rkc@kicet.re.kr
[b] Department of Materials Science & Engineering, Yonsei University, Seoul 120-749, Republic of Korea
[c] Nano Carbon Materials Research Group, Korea Electrotechnology Research Institute, Changwon 642-120, Republic of Korea
[d] School of Chemical Engineering, Sungkyunkwan University, Suwon 440–746 , Republic of Korea. E-mail: phs0727@skku.edu

† Electronic Supplementary Information (ESI) available: [HRTEM analysis, the STEM image of IL-C; N_2 adsorption/desorption isotherms, pore size distribution curves, XRD patterns and Raman spectra for IL-C; XPS wide-scan spectra of IL-C and IL-AC; Cyclic voltammetry curves of IL-AC; Capacitive performance of IL-C]. See DOI: 10.1039/b000000x/

1 A. S. Arico, P. Bruce, B. Scrosati, J.-M. Tarascon, and W. van Schalkwijk, *Nat. Mater.*, 2005, **4**, 366.
2 J. Lee, J. Kim and T. Hyeon, *Adv. Mater.*, 2006, **18**, 2073.
3 Y. Zhu, S. Murali, M. D. Stoller, K. J. Ganesh, W. Cai, P. J. Ferreira, A. Pirkle, R. M. Wallace, K. A. Cychosz, M. Thommes, D. Su, E. A. Stach and R. S. Ruoff, *Science*, 2011, **332**, 1537.
4 D. N. Futaba, K. Hata, T. Yamada, T. Hiraoka, Y. Hayamizu, Y. Kakudate, O. Tanaike, H. Hatori, M. Yumura and S. Iijima, *Nat. Mater.*, 2006, **5**, 987.
5 W. Xia, B. Qiu, D. Xia and R. Zou, *Sci. Rep.*, 2013, **3**, 1935.
6 N. P. Wickramaratne and M. Jaroniec, *ACS Appl. Mater. Interfaces*, 2013, **5**, 1849.
7 Z.-Z. Yang, Y.-N. Zhao and L.-N. *RSC Adv.*, 2011, **1**, 545.
8 N. Fechler, T.-P. Fellinger and M. Antonietti, *Adv. Mater.*, 2013, **25**, 75.
9 J. P. Paraknowitsch, J. Zhang, D. Su, A. Thomas and M. Antonietti, *Adv. Mater.*, 2010, **22**, 87.
10 J. P. Paraknowitsch, A. Thomas and M. Antonietti, *J. Mater. Chem.*, 2010, **20**, 6746.
11 J. S. Lee, X. Wang, H. Luo and S. Dai, *Adv. Mater.*, 2010, **22**, 1004.
12 S. Yuan, B. Dorney, D. White, S. Kirklin, P. Zapol, L. Yu and D.-J. Liu, *Chem. Commun.*, 2010, **46**, 4547.
13 P. K. Tripathi, M. Liu, Y. Zhao, X. Ma, L. Gan, O. Noonanb and C. Yub, *J. Mater. Chem. A*, 2014, **2**, 8534.
14 L. Qui, W. Chen, H. Xu, X. Xiong, Y. Jiang, F. Zou, X. Hu, Y. Xin, Z. Zhang and Y. Huang, *Energy Environ. Sci.*, 2013, **6**, 2497.
15 M. Choi and R. Ryoo, *Nat. Mater.*, 2003, **2**, 473.
16 D.-D. Zhou, Y.-J. Du, Y.-F. Song, Y.-G. Wang, C.-X. Wang and Y.-Y. Xia. *J. Mater. Chem. A*, 2013, **1**, 1192.
17 A. C. Ferrari and D. M. Basko, *Nat. Nanotechnol.*, 2013, **8**, 235.
18 P. Li, T.-J. Zhao, J.-H. Zhou, Z.-J. Sui, Y.-C. Dai, W.-K. Yuan, *Carbon*, 2005, **43**, 2701.
19 H. Wang, Z. Xu, A. Kohandehghan, Z. Li, K. Cui, X. Tan, T. J. Stephenson, C. K. King'ondu, C. M. B. Holt, B. C. Olsen, J. K. Tak, D. Harfield, A. O. Anyia and D. Mitlin, *ACS Nano*, 2013, **7**, 5131.
20 J. T. Han, B. H. Jeong, S. H. Seo, K. C. Roh, S. Kim, S. Choi, J. S. Woo, H. Y. Kim, J. I. Jang, D.-C. Shin, S. Jeong, H. J. Jeong, S. Y. Jeong and G.-W. Lee, *Nat. Commun.*, 2013, **4**, 2491.

